Seiichi Uchiyama* and Chie Gota

Luminescent molecular thermometers for the ratiometric sensing of intracellular temperature

DOI 10.1515/revac-2016-0021
Received June 17, 2016; accepted October 12, 2016; previously published online November 24, 2016

Abstract: Recently, numerous luminescent molecular thermometers that exhibit temperature-dependent emission properties have been developed to measure the temperatures of tiny spaces. Intracellular temperature is the most interesting and exciting applications of luminescent molecular thermometers because this temperature is assumed to be correlated with all cell events, such as cell division, gene expression, enzyme reaction, metabolism, and pathogenesis. Among the various types of temperature-dependent emission parameters of luminescent molecular thermometers, the emission intensity ratio at two different wavelengths is suitable for accurate and accessible intracellular temperature measurements. In this review article, luminescent molecular thermometers that exhibit a temperature-dependent emission intensity ratio in living cells are summarized, and current progress in intracellular thermometry is outlined.

Keywords: fluorescence; living cells; luminescence; probes; temperature.

Introduction

Temperature is the most important physical property of live cells. All biological reactions that are responsible for cellular functions are accompanied by heat release (exothermic) or heat absorption (endothermic), resulting in spatial temperature variation within the living cell. The local temperature variation could affect certain cellular functions, such as gene expression, protein stabilization, enzyme-ligand interactions, and enzyme activity (McCabe and Hernandez 2010, Inada and Uchiyama 2013) and *vice versa*. Therefore, intracellular thermometry could provide information regarding the status of the living cell. In medical studies using microcalorimetry, the cellular pathogenesis of diseases (e.g. cancer) was characterized by extraordinary heat production (Monti et al. 1986). Intracellular thermometry on a single-cell level should accelerate better understanding of cellular events and the development of novel diagnoses and therapies.

Among the potential thermometers for intracellular thermometry, luminescent molecular thermometers with temperature-dependent emission properties (e.g. intensity, wavelength, and lifetime) are promising tools due to their size being sufficiently small (i.e. nm order) compared to the size of living cells (Brites et al. 2012, Jaque and Vetrone 2012, Wang et al. 2013). In addition, their sensitivity to temperature variation has been greatly improved by the continuous efforts of many chemists (Uchiyama and Inada 2016). Very recently, the effects of protein kinase ASK1 on the thermogenesis of brown adipocytes were successfully evaluated on a single-cell level using a luminescent molecular thermometer (Hattori et al. 2016).

In intracellular thermometry using luminescent molecular thermometers, the observed emission intensity cannot be correlated to the temperature in a straightforward fashion. The emission intensity varies when the concentration of a luminescent molecular thermometer changes or the power of an excitation source (e.g. laser power) fluctuates (Valeur and Berberan-Santos 2012). Therefore, the accuracy of intracellular thermometry decreases if the emission intensity is adopted as a temperature-dependent parameter. However, the emission intensity ratio at two different wavelengths or the emission lifetime is a suitable parameter for accurate intracellular thermometry. In particular, ratiometric intracellular thermometry that is conducted by measuring the emission intensity ratio is advantageous in terms of accessibility to measurement equipment (i.e. common fluorescence microscope) and high temporal resolution (i.e. better than 1 s) (Uchiyama et al. 2015). Although the ratiometric sensing advantages allow for imaging ions and molecules inside living cells (Lee et al. 2015), they also apply to ratiometric intracellular thermometry. Most luminescent molecular thermometers used in ratiometric intracellular thermometry provide emission intensity ratios via a single excitation at a fixed wavelength. More conveniently, all of the ratiometric luminescent molecular thermometers can enter living cells either by their own ability or with the

***Corresponding author: Seiichi Uchiyama,** Graduate School of Pharmaceutical Sciences, The University of Tokyo, 7-3-1 Hongo Bunkyo-ku, 113-0033 Tokyo, Japan,
e-mail: seiichi@mol.f.u-tokyo.ac.jp
Chie Gota: Graduate School of Pharmaceutical Sciences, The University of Tokyo, 7-3-1 Hongo Bunkyo-ku, 113-0033 Tokyo, Japan

support of additional cationic polymers. Therefore, users who intend to measure intracellular temperature are not hindered by cumbersome experimental procedures (e.g. microinjection) using the developed ratiometric luminescent molecular thermometers. Here, we provide an overview of ratiometric luminescent molecular thermometers that have been utilized in intracellular thermometry. Table 1 provides a summary, and each case will be outlined in the following sections.

Responses of ratiometric luminescent molecular thermometers

Most ratiometric luminescent thermometers use emission intensities at two different wavelengths (I_1 at λ_1 and I_2 at λ_2) to afford a temperature-dependent emission intensity ratio (I_1/I_2). Figure 1A–C illustrates the classification of the temperature-dependent emission spectra of ratiometric luminescent molecular thermometers. In type A, the maximum emission wavelength shifts with variation in temperature. Only a few cases (e.g. quantum dots) indicate the emission spectra observed in type A. In type B, emission intensity at one wavelength (λ_1) is temperature dependent, while that at another wavelength (λ_2) is constant regardless of temperature. If ratiometric luminescent molecular thermometers consisted of two lumophores that radiate temperature-dependent and temperature-independent (i.e. reference) emissions, then the emission spectra would follow that of type B. In type C, an emission intensity at one wavelength (λ_1) decreases with changes in temperature (T_1 to T_2), whereas that at another wavelength (λ_2) simultaneously increases. If a lumophore has two emissive states that are thermally equilibrated, the emission spectra comply with that of type C. Moreover, when ratiometric luminescent molecular thermometers consist of two lumophores, and temperature-dependent energy transfer between them is involved, the emission spectra follow that of type C. The response types of each ratiometric luminescent molecular thermometer are indicated in Table 1.

Ratiometric luminescent molecular thermometers

Small organic molecules

Over 20 years ago, a polarity-sensitive fluorescent compound having an intramolecular charge transfer character (i.e. 6-dodecanoyl-2-dimethylamino-naphthalene [laurdan], Figure 2A) was used for cellular thermometry (Chapman et al. 1995). The plasma membranes of Chinese hamster ovary (CHO) cells undergo a gel-to-liquid crystalline phase transition as the temperature increases, and therefore, the local polarity near the plasma membrane increases. Due to its high hydrophobicity, laurdan can be localized in the plasma membrane to sense this heat-induced change in the local polarity, which results in a small shift in the fluorescence spectrum (Figure 2B). According to the categorization into type A as illustrated in Figure 1, the ratio calculated from the fluorescence intensities of laurdan at 440 nm and 490 nm is temperature dependent (Figure 2C). Although the temperature resolution of laurdan was relatively low (i.e. lower than 1°C), and no further biological experiments were conducted in the original work, this study was the first report to correlate the cellular temperature with the temperature-dependent luminescence properties of a lumophore.

In general, the sensitivities of small organic molecules to changes in temperature are too low to be applied in cellular thermometry. Rhodamine B (Figure 3) is one of the most sensitive small organic molecules, and this compound in the zwitterion open form exhibits heat-induced fluorescence quenching due to the rotation of the diethylamino group and subsequent nonradiative internal conversion (estimated activation energy = 26 kJ/mol) (Snare et al. 1982). Therefore, rhodamine B has been extensively utilized in the thermometry of nonbiological subjects (e.g. microfluidic systems). Nevertheless, the use of rhodamine B in cellular thermometry has been questioned because it is undesirably affected by environmental changes, such as pH changes and protein denaturation (Paviolo et al. 2013). This challenge has been avoided via the use of the ratiometric fluorescent molecular thermometer Mito-RTP, in which a carboxylic group of rhodamine B is connected to a temperature-insensitive reference fluorophore, CS NIR, through a hexylene linker (Figure 4A) (Homma et al. 2015). Mito-RTP stained the mitochondria of human epithelial carcinoma (HeLa) cells within 30 min (Figure 4B), and the fluorescence intensity ratio of the rhodamine B moiety to the CS NIR moiety in Mito-RTP decreased as the cellular temperature increased (Figure 4C). The disadvantage of using Mito-RTP is that different excitations (at 563 nm and 722 nm) are required to obtain the fluorescence intensities of the rhodamine B and CS NIR moieties. With a high temperature resolution (0.6°C), Mito-RTP was successfully employed to monitor the significant increase in the mitochondrial temperature due to an external stimulus using an uncoupler agent [i.e. carbonyl cyanide 4-(trifluoromethoxy)phenylhydrazone, FCCP] (Figure 4D).

Table 1: Ratiometric luminescent molecular thermometers for cellular thermometry.

Thermometer (response type[a])	Commercially available	Excitation (nm)	Emission (nm)	Tested cell line	Introduction into cells	Distribution within cells	T res. (°C)[b]	Ref.
Small organic molecules								
Laurdan (A)	Yes	365	440, 490	CHO	Incubation at 37°C for 35 min	Mainly cell membrane	1	Chapman et al. 1995
Mito-RTP (B)	No	563, 722	587, 756	HeLa	Incubation at 37°C for 30 min	Mitochondria	0.6	Homma et al. 2015
Lumophore(s)-labeled thermoresponsive synthetic polymers								
Poly(NNPAM-*co*-APTMA-*co*-DBThD-*co*-BODIPY) (B)	Yes	458	515, 580	MOLT-4, HEK293T	Incubation at 25°C for 10 min	Whole cell	0.01–1	Uchiyama et al. 2015
Poly(NNPAM-*co*-APTMA-*co*-Ir_1-*co*-Ir_2) (partially B)	No	405	485, 595	HeLa, zebrafish larva	Incubation at 25°C for 2 h (for HeLa)	Cytoplasm	–	Chen et al. 2016
Poly(NIPAM-*co*-NBD) and poly(NIPAM-*co*-Rh) (B)	No	488	535, 620	HeLa	Incubation at 28°C for 3 h	Cytoplasm	0.3–0.5	Qiao et al. 2014
Nile red containing poly(NIPAM-*co*-DPTB) nanogel (B)	No	405	475, 625	NIH/3T3	Incubation at 37°C for 30 min	Cytoplasm	–	Liu et al. 2015
PEG-*b*-(NIPAM-*co*-CMA), PEG-*b*-(NIPAM-*co*-NBDAE) and PEG-*b*-(NIPAM-*co*-RhBEA) (C)	No	405	430, 585	HepG2	Incubation at 37°C for 40 min	Cytoplasm	0.4	Hu et al. 2015
Poly(NIPAM-*co*-NBD-*co*-TfAuNC) (B)	No	488	535, 620	HeLa	Incubation at 25°C for 3 h	Cytoplasm	0.3–0.5	Qiao et al. 2015
Polymeric materials containing temperature-sensitive lumophores								
PS-RhB containing PFBT nanoparticle (B)	No	458	513, 577	HeLa	Via endocytosis	Partially within a cell	–	Ye et al. 2011
Eu-TTA and rhodamine 101 containing RFNT (B)	No	360, 545	598, 629	HeLa	Incubation at 37°C for 2 h	Endosome	1.0	Takei et al. 2014
EuDT and $Ir(ppy)_3$ containing PS-RNT (B)	No	405	540, 620	Fruit fly larva	Oral dose	–	1.0–1.7	Arai et al. 2015
Eu^{3+} and Tb^{3+} containing P4VP-*b*-P(MPEGA-*co*-PEGA) (B)	No	365	545, 610	OK	Incubation for 24 h	Mostly nucleus	0.5	Piñol et al. 2015
Polyethylenimine coated $NaYF_4$:Er^{3+},Yb^{3+} nanoparticle (B)	No	920	525, 545	HeLa	Incubation for 1.5 h	Dotted within a cell	–	Vetrone et al. 2010
GFP								
tsGFP1 (C)	No	405, 488	510	HeLa, brown adipocyte, myotube	Genetically expressed	Cytoplasm, and targeted to mitochondria and ER	–	Kiyonaka et al. 2013
Quantum dots and carbon dots								
Qdot 655 (A)	Yes	405	640, 660	SH-SY5Y	37°C for 1 h, assisted by a peptide	Dotted in cytoplasm	–	Tanimoto et al. 2016
Quantum dot/quantum rod complex (partially B)	No	400	635, 669	HeLa	Assisted by a cationic polymer	–	–	Albers et al. 2012
Carbon dot/gold nanocluster hybrid (B)	No	365	435, 600	Fixed HEK293T	Incubation at 37°C for 2 h	–	–	Wang et al. 2016

[a]See Figure 1 and "Responses of ratiometric luminescent molecular thermometers" section. [b]Temperature resolution.

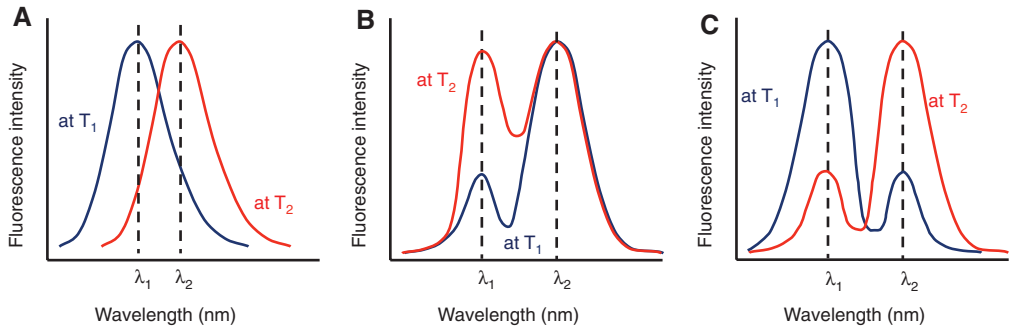

Figure 1: Temperature-dependent emission spectra of ratiometric luminescent molecular thermometers. (A)–(C) represent different types of responses at two temperatures (T_1 and T_2).

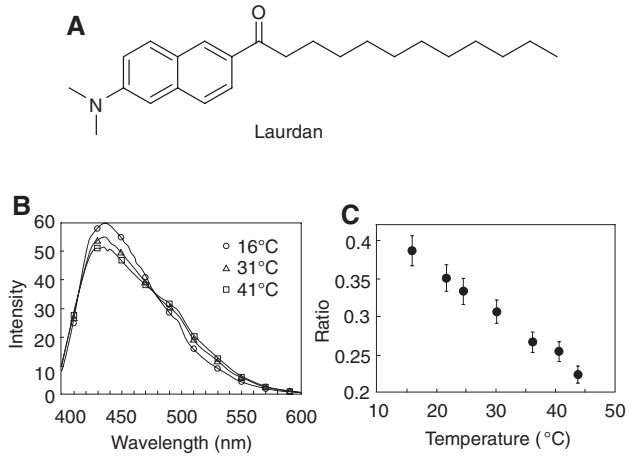

Figure 2: Temperature-sensitive fluorescence of laurdan located in the plasma membrane.
(A) Chemical structure of laurdan. (B) Fluorescence spectra of laurdan located in the plasma membrane of living CHO cells in suspension (λ_{ex} = 365 nm). (C) Relationship between the ratios calculated from the fluorescence intensities (FIs) and the temperature of CHO cells. The ratio value equals (FI at 440 nm – FI at 490 nm)/(FI at 440 nm + FI at 490 nm). Reproduced with permission from Chapman et al. (1995). Copyright 1995 John Wiley and Sons.

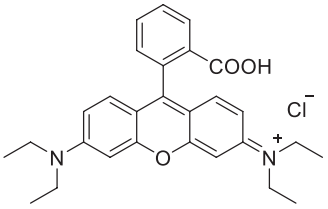

Figure 3: Chemical structure of rhodamine B.

Lumophore(s)-labeled thermoresponsive synthetic polymers

In 2003, we established a general design for developing a highly sensitive fluorescent thermometer that works in an aqueous solution by combining a thermo-responsive polymer and a polarity- and hydrogen bonding-sensitive fluorophore (Uchiyama et al. 2003). For example, a copolymer consisting of *N*-isopropylacrylamide (NIPAM) and 4-*N*-(2-acryloyloxyethyl)-*N*-methylamino-7-*N*,*N*-dimethylaminosulfonyl-2,1,3-benzoxadiazole (DBD) [poly(NIPAM-*co*-DBD), Figure 5A] in water undergoes a temperature-induced phase transition at approximately 32°C. Below 32°C, the main chain of poly(NIPAM-*co*-DBD) becomes extended with hydration. In this situation, the DBD units in poly(NIPAM-*co*-DBD) are weakly fluorescent because the fluorophore (DBD) is strongly quenched by water molecules (Figure 5B) (Gota et al. 2008). In contrast, the copolymer folds into a contracted structure above 32°C, and water molecules become remote from the main chain. Then, the polarity- and hydrogen bonding-sensitive DBD units in the copolymer become fluorescent. Thus, poly(NIPAM-*co*-DBD) exhibited a 13.3-fold stronger fluorescence at 37°C compared to that at 29°C (Figure 5C), which was viewed as an unusual fluorescence behavior because increases in temperature for small organic and inorganic molecules can generally accelerate only non-radiative relaxation processes and reduce their emission intensities (Uchiyama et al. 2006). This strategy, i.e. combining a thermo-responsive polymer and a polarity- and hydrogen bonding-sensitive fluorophore, has been widely adopted by many research groups for the development of fluorescent polymeric thermometers and can be applied to create ratiometric fluorescent polymeric thermometers by introducing another reference fluorophore that is insensitive to polarity and hydrogen bonding or by introducing a paired structure for electron/energy transfer to/from the first polarity- and hydrogen bonding-sensitive fluorophore.

A copolymer consisting of *N*-*n*-propylacrylamide (NNPAM), (3-acrylamidopropyl)trimethylammonium chloride (APTMA), *N*-(2-{[7-(*N*,*N*-dimethylaminosulfonyl)-2,1,3-benzothiadiazol-4-yl]-(methyl)amino}ethyl)-*N*-

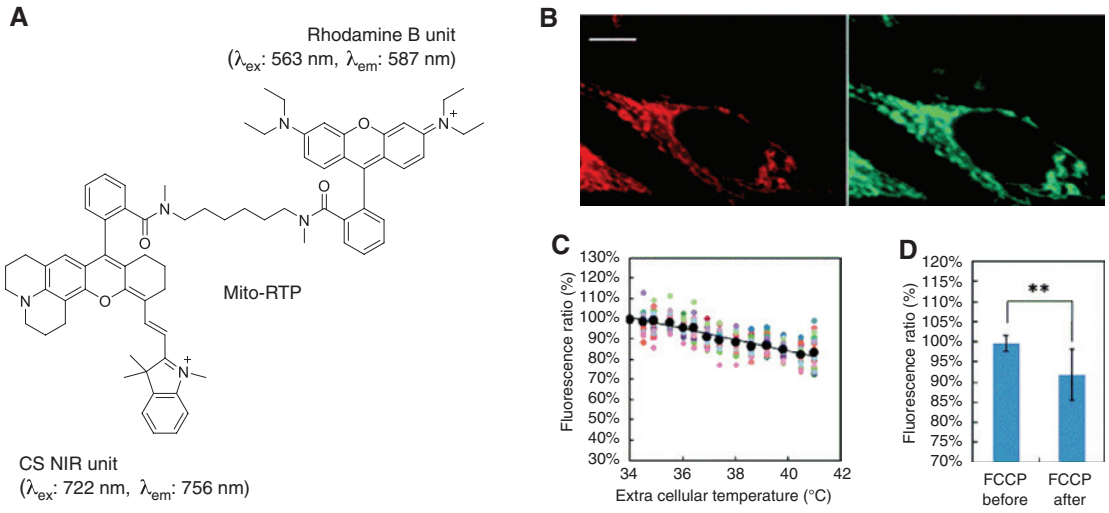

Figure 4: Measurement of mitochondrial temperature using Mito-RTP.
(A) Chemical structure of Mito-RTP that consists of rhodamine B and CS NIR units. (B) Localization of Mito-RTP. Fluorescence images of Mito-RTP (left) and mito-tracker green (right). Scar bar = 5 μm. (C) Temperature-dependent fluorescence intensity ratio (rhodamine B unit/CS NIR unit) of Mito-RTP in living HeLa cells. The colored and black markers represent individual measurements (n = 26) and their averages, respectively. (D) Change in the fluorescence intensity ratio as a function of chemical stimuli using FCCP. **$p = 8.1 \times 10^{-5}$ using Student's t-test before (– 90 s) and after (330 s) addition of FCCP. Reproduced with permission from Homma et al. (2015). Copyright 2015 Royal Society of Chemistry.

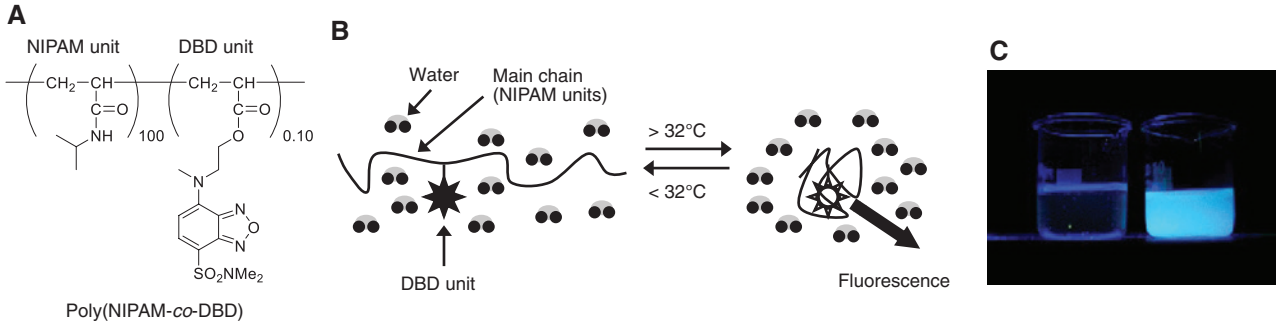

Figure 5: Highly sensitive fluorescent polymeric thermometer.
(A) Chemical structure of poly(NIPAM-*co*-DBD). (B) Functional mechanism of poly(NIPAM-*co*-DBD). (C) Fluorescence photograph of poly(NIPAM-*co*-DBD) ($M_w = 39{,}400$, $M_n = 27{,}600$, $M_w/M_n = 1.43$) in water (left: cold, right: hot).

methylacrylamide (DBThD), and 8-(4-acrylamidophenyl)-4,4-difluoro-1,3,5,7-tetramethyl-4-bora-*3a*,*4a*-diaza-*s*-indacene (BODIPY) [poly(NNPAM-*co*-APTMA-*co*-DBThD-*co*-BODIPY)] (Figure 6A) was our version of a ratiometric fluorescent polymeric thermometer for sensing intracellular temperature (Uchiyama et al. 2015). The NNPAM units are thermoresponsive and undergo a heat-induced structural change, and the APTMA units increase the solubility of the copolymer and support its spontaneous entry into living cells. Because the DBThD units are polarity- and hydrogen bonding-sensitive fluorophores, and because the BODIPY units are polarity- and hydrogen bonding-insensitive fluorophores, the DBThD and BODIPY units exhibit temperature-dependent and temperature-independent fluorescence, respectively, when poly(NNPAM-*co*-APTMA-*co*-DBThD-*co*-BODIPY) is dissolved in an aqueous solution. After incubation of MOLT-4 (human acute lymphoblastic leukemia) or HEK293T (human embryonic kidney) cells with the copolymer at 25°C for 10 min, the temperature-dependent fluorescence spectra can be observed from the whole cells (Figure 6B–E). The temperature resolution of the polymeric thermometer depended on the experimental apparatus (e.g. a spectrofluorimeter or fluorescence microscope) and reached 0.01–0.25°C when a spectrofluorimeter was used.

Recently, a similar luminescent polymeric thermometer [i.e. poly(NNPAM-*co*-APTMA-*co*-Ir_1-*co*-Ir_2) that consists of the same NNPAM and APTMA units but different

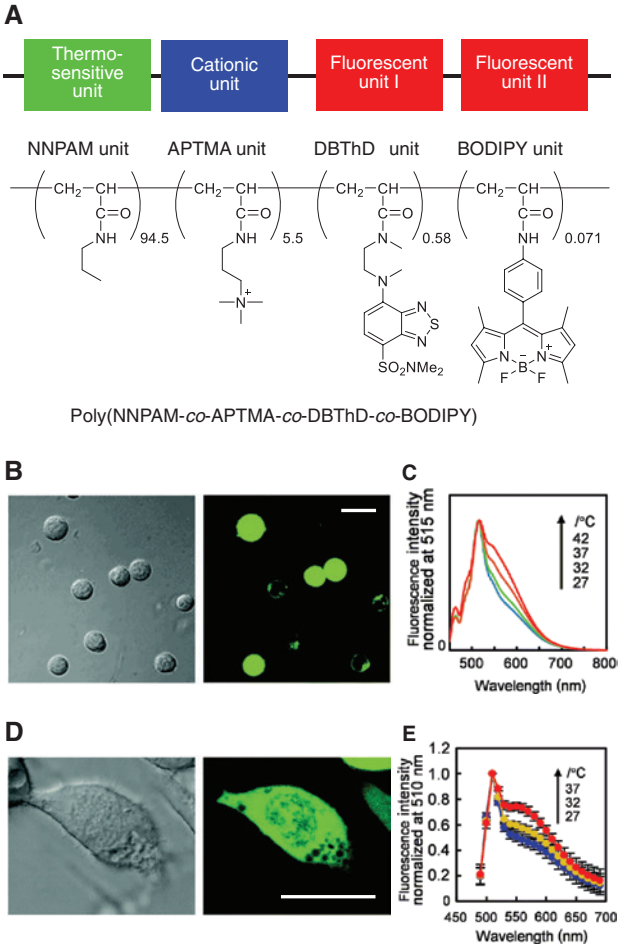

Figure 6: Intracellular thermometry of living mammalian cells using ratiometric poly(NNPAM-*co*-APTMA-*co*-DBThD-*co*-BODIPY) (M_w = 20,300, M_n = 10,800, M_w/M_n = 1.88).
(A) Chemical structure of poly(NNPAM-*co*-APTMA-*co*-DBThD-*co*-BODIPY). (B) Representative images of MOLT-4 cells treated with poly(NNPAM-*co*-APTMA-*co*-DBThD-*co*-BODIPY). Differential interference contract (DIC) image (left) and confocal fluorescence image (right). Scar bar = 20 μm. (C) Fluorescence spectra of poly(NNPAM-*co*-APTMA-*co*-DBThD-*co*-BODIPY) in living MOLT-4 cells at 27, 32, 37, and 42°C (λ_{ex} = 458 nm). (D) Representative images of HEK293T cells treated with poly(NNPAM-*co*-APTMA-*co*-DBThD-*co*-BODIPY). DIC image (left) and confocal fluorescence image (right). Scar bar = 20 μm. (E) Averaged fluorescence spectra of poly(NNPAM-*co*-APTMA-*co*-DBThD-*co*-BODIPY) in a single HEK293T cell (n = 9, mean ± SD) at 27, 32, and 37°C (λ_{ex} = 473 nm). Reproduced with permission from Uchiyama et al. (2015). Copyright 2015 Royal Society of Chemistry.

luminescent Ir_1 and Ir_2 units bearing iridium complexes] was reported (Figure 7A) (Chen et al. 2016). When introduced into the copolymer, both the Ir_1 and Ir_2 units exhibited luminescence enhancement with increasing temperature due to the increases in the rigidities of the iridium complexes and the decreases in their surrounding polarities. Notably, the maximum luminescence wavelength and the magnitude of the luminescence enhancement differ between the Ir_1 and Ir_2 units. Thus, the emission intensity ratio [$R(I_{470}/I_{590})$] of the two Ir units was temperature dependent in PBS (pH 7.4) with a moderate temperature resolution (0.5°C) (Figure 7B and C). This temperature-dependent luminescent property of poly(NNPAM-*co*-APTMA-*co*-Ir_1-*co*-Ir_2) was also confirmed in living HeLa cells (Figure 7D) and even in microinjected zebrafish larvae (Figure 7E). Although the novelty of this polymeric sensor is related to the temperature-dependent phosphorescence lifetime of the Ir units, it is important to include this sensor in this review article.

Although the sensing system becomes more complicated, a combination of poly(NIPAM-*co*-NBD) (NBD: nitrobenzoxadiazole) and poly(NIPAM-*co*-Rh) (Rh: rhodamine derivative) (Figure 8A) has been applied for the ratiometric sensing of intracellular temperature (Qiao et al. 2014). Based on the abilities of the NBD units to sense water molecules in their surrounding environment, poly(NIPAM-*co*-NBD) exhibited temperature-dependent fluorescence (Uchiyama et al. 2003). On the other hand, poly(NIPAM-*co*-Rh) exhibited temperature-independent fluorescence because the Rh units lack sensitivity to water molecules. In contrast to rhodamine B, the Rh units themselves are not sensitive to temperature variations, probably due to the closed form. Therefore, a temperature-dependent fluorescence intensity ratio can be obtained from a mixture of poly(NIPAM-*co*-NBD) and poly(NIPAM-*co*-Rh) in biological cells when the spatial distributions of these copolymers are identical inside the cells. Based on this assumption, the intracellular temperatures of living HeLa cells were monitored using a mixture of poly(NIPAM-*co*-NBD) and poly(NIPAM-*co*-Rh) to achieve a temperature resolution of 0.3–0.5°C (Figure 8B and C). FCCP-induced temperature increases of HeLa cells were also detected using these copolymers (Figure 8D).

A mixture of poly(NIPAM-*co*-dipyren-1-yl(2,4,6-triisopropylphenyl)borane) nanogel (poly(NIPAM-*co*-DPTB) nanogel) and Nile red has been used for ratiometric intracellular thermometry (Figure 9A) (Liu et al. 2015). Poly(NIPAM-*co*-DPTB) nanogel containing an environmentally sensitive DPTB unit changes its size and fluorescence properties as a function of temperature variations. The detailed mechanism of the fluorescence enhancement of poly(NIPAM-*co*-DPTB) nanogel at higher temperatures is unclear but is thought to be the result of the decrease in the local polarity near the DPTB units and/or the increase in rigidity of the DPTB units, which are caused by a heat-induced intramolecular association of the NIPAM units. The Nile red molecules dispersed in the poly(NIPAM-*co*-DPTB) nanogel can interact with the DPTB unit via Förster

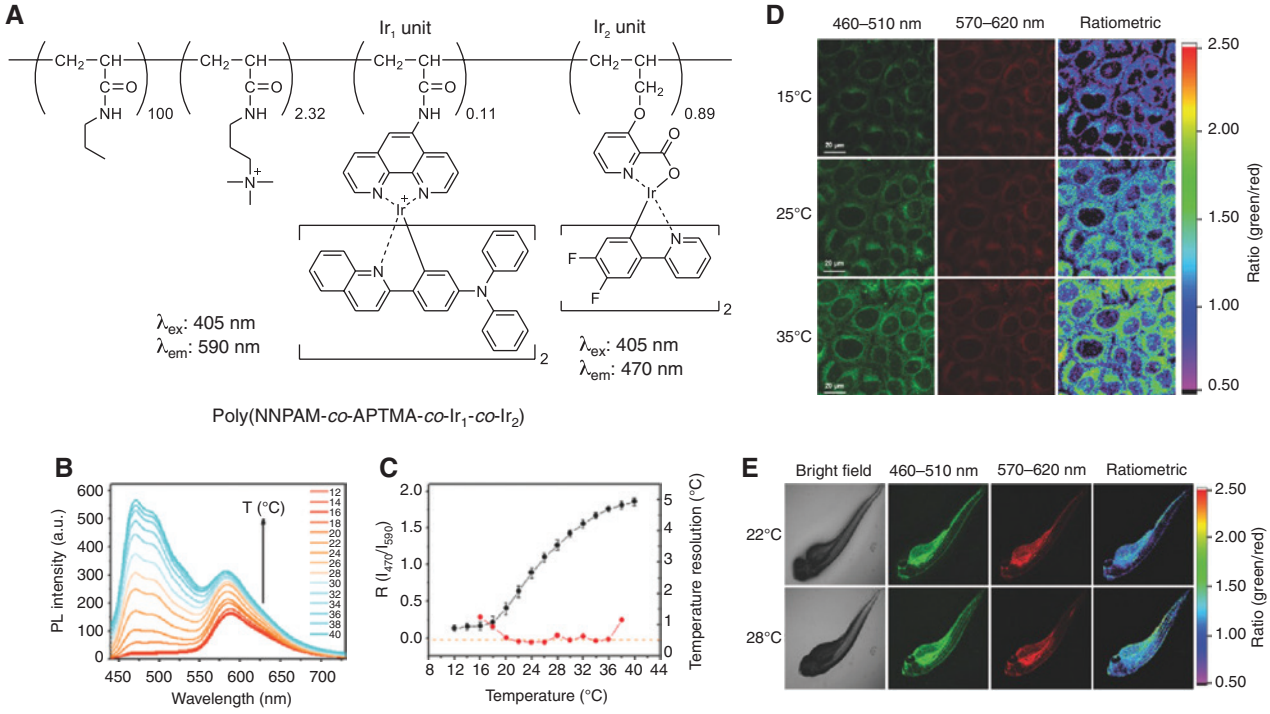

Figure 7: *In vivo* temperature sensing using poly(NNPAM-*co*-APTMA-*co*-Ir_1-*co*-Ir_2) ($M_w = 20{,}700$, $M_n = 10{,}100$, $M_w/M_n = 2.05$). (A) Chemical structure of poly(NNPAM-*co*-APTMA-*co*-Ir_1-*co*-Ir_2). (B) Photoluminescence (PL) spectra of poly(NNPAM-*co*-APTMA-*co*-Ir_1-*co*-Ir_2) (0.01 w/v%) in a PBS buffer (pH 7.4) ($\lambda_{ex} = 405$ nm). (C) Temperature-dependent photoluminescence intensity ratio at 470 and 590 nm [$R(I_{470}/I_{590})$, black, left axis] in a PBS buffer (pH 7.4) and corresponding temperature resolution (red, right axis). (D) Phosphorescence images of living HeLa cells that were labeled with poly(NNPAM-*co*-APTMA-*co*-Ir_1-*co*-Ir_2) (left and center) and the corresponding ratiometric images (right) ($\lambda_{ex} = 405$ nm). (E) Bright field images (leftmost), phosphorescence images (second and third from the left, $\lambda_{ex} = 405$ nm), and the corresponding ratiometric images (rightmost) of living zebrafish larva after microinjection of poly(NNPAM-*co*-APTMA-*co*-Ir_1-*co*-Ir_2). Reproduced with permission from Chen et al. (2016). Copyright 2016 John Wiley and Sons.

resonance energy transfer (FRET) and emit a reference fluorescence when the DPTB units are excited. This functional mechanism worked in an aqueous solution (Figure 9B) and in NIH/3T3 (mouse embryonic fibroblast) cells, although quantitative data are not shown (Figure 9C).

A mixture of three block copolymers consisting of poly(ethylene glycol) (PEG) units and fluorescent poly(NIPAM) units exhibited a sequential FRET-based temperature-dependent fluorescence signal in HepG2 (human Caucasian hepatocellular carcinoma) cells (Hu et al. 2015). The first FRET occurs from the block copolymer labeled with coumarin (CMA) [i.e. PEG-*b*-P(NIPAM-*co*-CMA) in Figure 10A] to that labeled with the acryloyl ester of NBD (NBDAE) [i.e. PEG-*b*-P(NIPAM-*co*-NBDAE)]. The second FRET can occur from PEG-*b*-P(NIPAM-*co*-NBDAE) to the block copolymer labeled with the acryloyl ester of rhodamine B (RhBEA) [i.e. PEG-*b*-P(NIPAM-*co*-RhBEA)] when the excited state of PEG-*b*-P(NIPAM-*co*-NBDAE) is emissive. Because PEG-*b*-P(NIPAM-*co*-NBDAE) fluoresces more strongly at higher temperatures, the second FRET is accelerated by increasing the temperature. As a result, the fluorescence intensity ratio of PEG-*b*-P(NIPAM-*co*-CMA) (emission: 410–450 nm) and PEG-*b*-P(NIPAM-*co*-RhBEA) (emission: 565–605 nm) changes due to temperature variations (Figure 10B and C). The highest temperature resolution of this system was 0.4°C at 37°C.

A copolymer consisting of NIPAM, NBD, and transferrin protein-stabilized fluorescent gold nanocluster (TfAuNCs) units [poly(NIPAM-*co*-NBD-*co*-TfAuNC)] is another ratiometric luminescent polymeric thermometer (Qiao et al. 2015). Poly(NIPAM-*co*-NBD-*co*-TfAuNC) was prepared by introducing TfAuNCs into the *N*-succinimide *p*-vinylbenzoate (NSVB) units of poly(NIPAM-*co*-NBD-*co*-NSVB) (Figure 11A). The thermoresponsive NIPAM units and environmentally sensitive NBD units resulted in a change in the fluorescence intensity at 545 nm as the temperature varies according to the general strategy for designing sensitive fluorescent polymeric thermometers described above (Figure 11B). The TfAuNC moiety in poly(NIPAM-*co*-NBD-*co*-TfAuNC) helped to target cells and emitted the reference luminescence signals at 659 nm. Although 3 h was required to enter the HeLa cells,

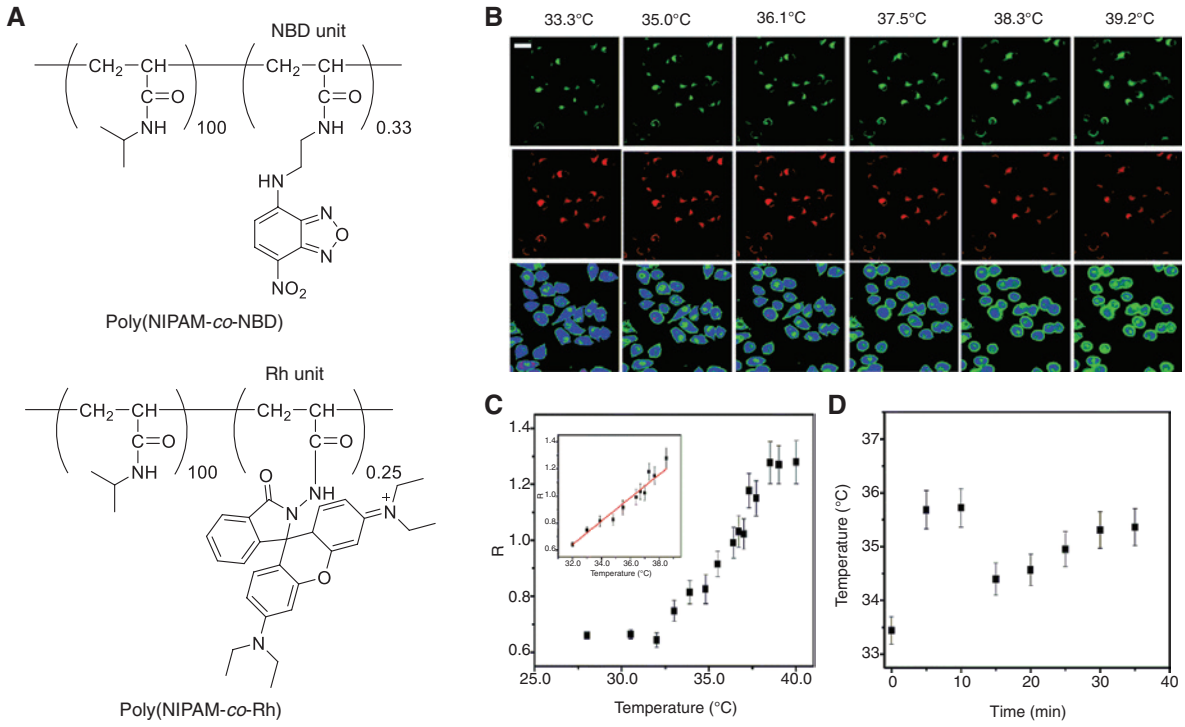

Figure 8: Intracellular thermometry of living HeLa cells with a combination of two poly(NIPAM) copolymers.
(A) Chemical structures of poly(NIPAM-*co*-NBD) (M_n = 11,062) and poly(NIPAM-*co*-Rh) (M_n = 9896). (B) Fluorescence images of poly(NIPAM-*co*-NBD) and poly(NIPAM-*co*-Rh) in living HeLa cells at different temperatures. The images in the first row and the second row were collected in the range of 510–560 nm and 570–670 nm, respectively. The images in the third row were of the ratio of the first and second images. Scar bar = 20 μm. (C) Temperature-dependent fluorescence intensity ratio (R) obtained from the images shown in panel B. Inset: Calibration line for intracellular thermometry. (D) Change in intracellular temperature of HeLa cells after the chemical stimuli with FCCP. Reproduced with permission from Qiao et al. (2014). Copyright 2014 Royal Society of Chemistry.

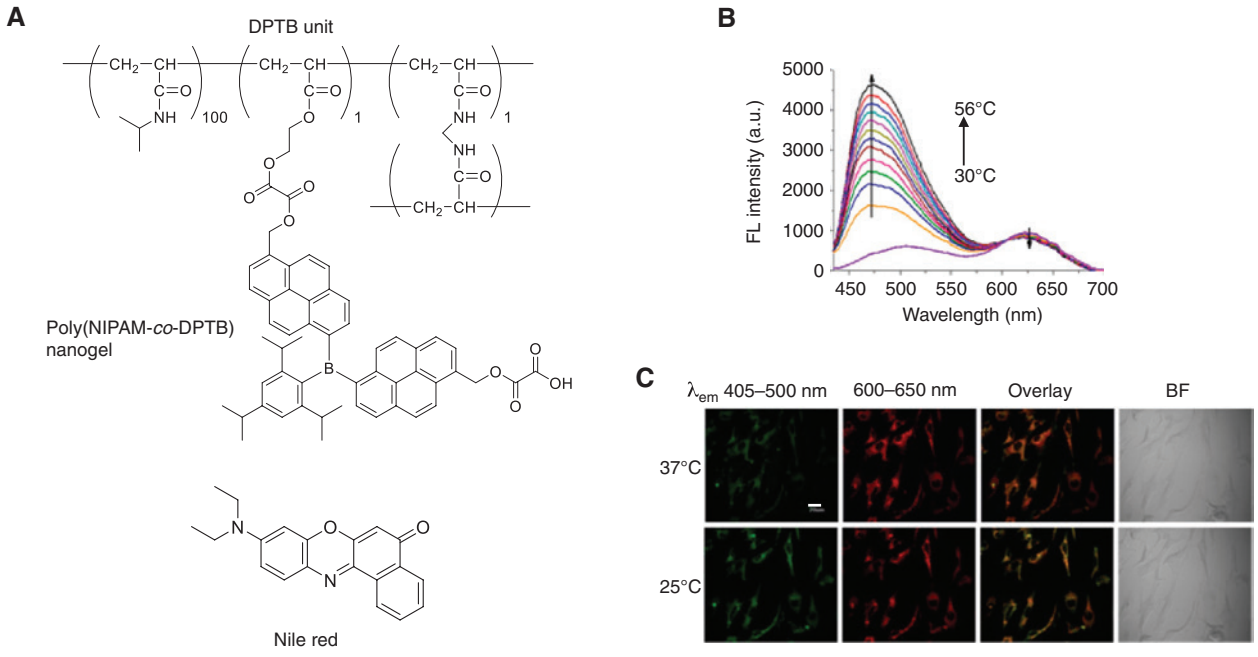

Figure 9: Ratiometric temperature sensing system composed of poly(NIPAM-*co*-DPTB) nanogel and Nile red.
(A) Chemical structures of poly(NIPAM-*co*-DPTB) nanogel and Nile red. (B) Fluorescence spectra of a mixture of poly(NIPAM-*co*-DPTB) nanogel and Nile red in water (0.5 mg/ml in total) (λ_{ex} = 405 nm). (C) Confocal fluorescence images (leftmost and second), their overlay images (third from the left), and bright field (BF) images (rightmost) of NIH/3T3 cells labeled with poly(NIPAM-*co*-DPTB) nanogel and Nile red (λ_{ex} = 405 nm). Reproduced with permission from Liu et al. (2015). Copyright 2015 American Chemical Society.

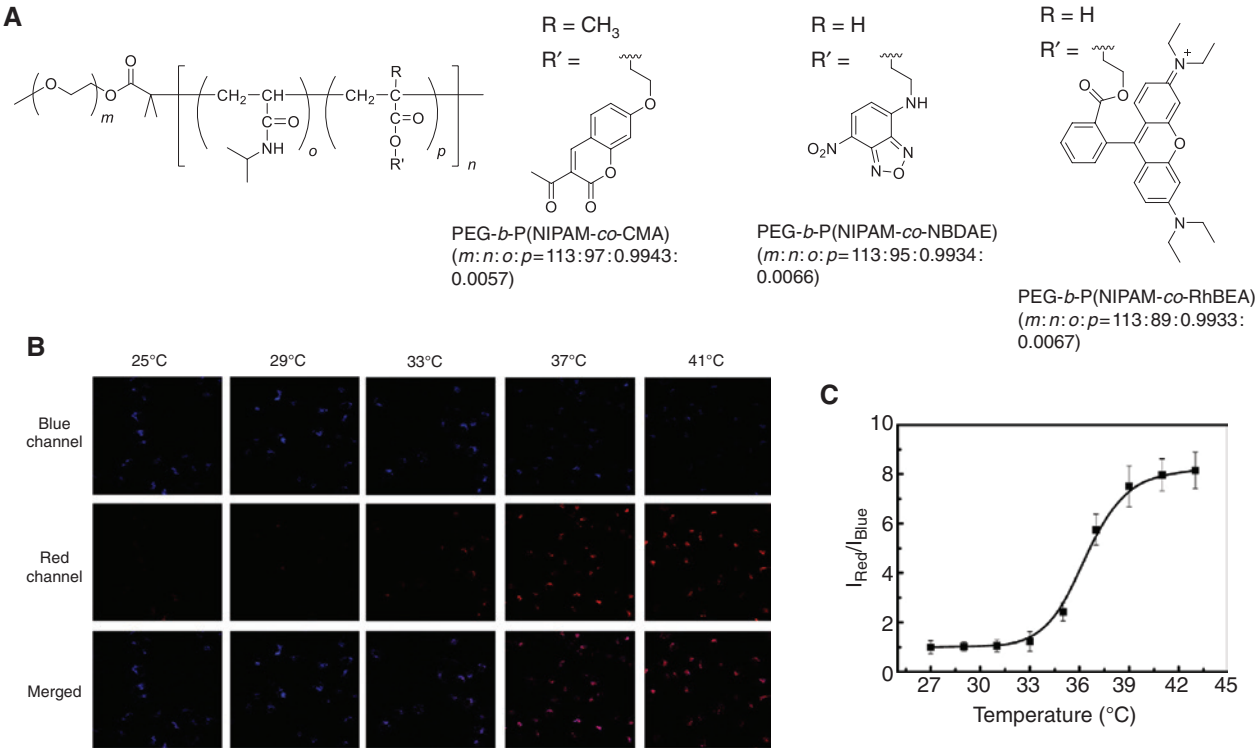

Figure 10: FRET-based ratiometric fluorescent thermometers for intracellular thermometry.
(A) Chemical structures of PEG-*b*-P(NIPAM-*co*-CMA) (M_n = 15.4 kDa), PEG-*b*-P(NIPAM-*co*-NBDAE) (M_n = 15.8 kDa) and PEG-*b*-P(NIPAM-*co*-RhBEA) (M_n = 14.9 kDa). (B) Confocal fluorescence images of HepG2 cells incorporating the three polymeric thermometers (blue channel: 410–450 nm, red channel: 565–605 nm) and their merged images at different temperatures (λ_{ex} = 405 nm). (C) Relationship between the fluorescence intensity ratio of the two channels (I_{Red}/I_{Blue}) and the temperature. Reproduced with permission from Hu et al. (2015). Copyright 2015 American Chemical Society.

poly(NIPAM-*co*-NBD-*co*-TfAuNC) exhibited a temperature-dependent emission intensity ratio in living HeLa cells with a high temperature resolution (0.3–0.5°C) (Figure 11C and D). Time-lapse monitoring of the intracellular temperature of HeLa cells was performed after application of a chemical stimulus (i.e. ionomycin calcium complex), which induced a Ca^{2+} shock (Figure 11E).

Polymeric materials containing temperature-sensitive lumophores

Polymeric particles are good materials for supporting a temperature-sensitive lumophore. Once supported in polymeric particles, a temperature-sensitive lumophore can be protected from chemical decomposition and undesirable photophysical interactions with molecules surrounding the polymeric particles. If a temperature-insensitive lumophore is also embedded into the polymeric particles, the ratio of the emission intensities of the two lumophores is expected to be temperature-sensitive. The difference in the polymeric luminescent molecular thermometers between the "Lumophore(s)-labeled thermoresponsive synthetic polymers" and this section is in the design and the origin of function; the sensitivity to temperature variation is attributable to lumophores in the ratiometric luminescent molecular thermometers outlined in this section, but is based on polymers in the ratiometric luminescent molecular thermometers described in the "Lumophore(s)-labeled thermoresponsive synthetic polymers" section.

Fluorescent poly[(9,9-dioctylfluorenyl-2,7-diyl)-*co*-(1,4-benzo-{2,1′,3}-thiadiazole)] (PFBT) nanoparticles containing rhodamine B-labeled polystyrene (PS-RhB) have been used as a ratiometric luminescent thermometer (Figure 12A) (Ye et al. 2011). As described in the "Small organic molecules" section, the rhodamine B moiety in PS-RhB exhibited temperature-dependent fluorescence intensity at approximately 570 nm. PFBT is fluorescent at 510 nm and is also capable of transferring a part of the excited energy to the temperature-sensitive rhodamine B structure. Thus, the fluorescence intensity ratio of the PFBT nanoparticles containing PS-RhB at 510 nm and 573 nm in an aqueous solution was temperature dependent (Figure 12B and C). In the original study, the fluorescence images of the nanoparticles in HeLa cells were acquired at two different temperatures to demonstrate

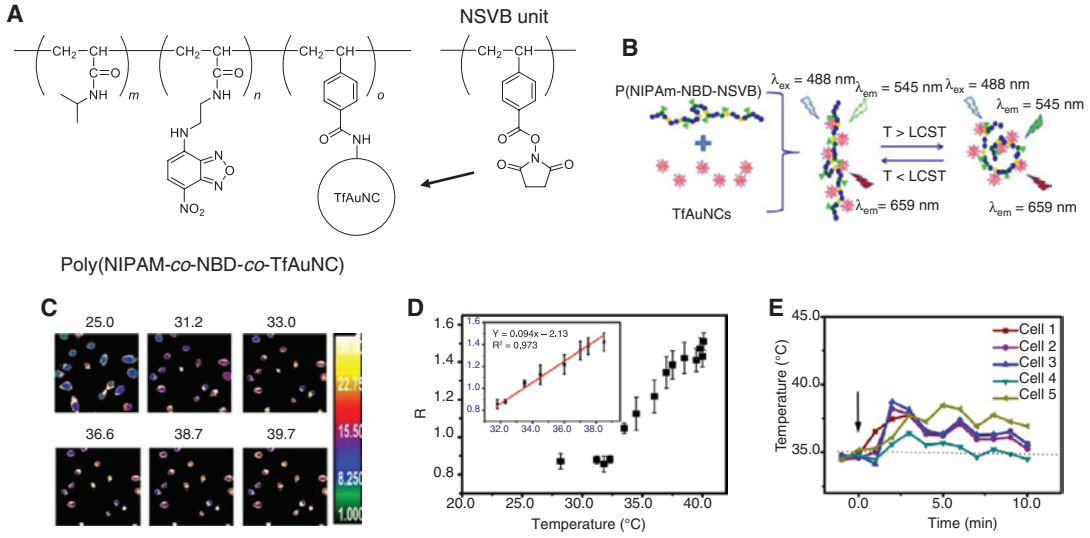

Figure 11: Intracellular thermometry of living HeLa cells using poly(NIPAM-*co*-NBD-*co*-TfAuNC).
(A) Chemical structures of poly(NIPAM-*co*-NBD-*co*-TfAuNC) and NSVB units. (B) Schematic representation of the function of poly(NIPAM-*co*-NBD-*co*-TfAuNC). When heated at temperatures higher than the lower critical solution temperature (LCST), the three-dimensional structure of poly(NIPAM-*co*-NBD-*co*-TfAuNC) changes from an open form to a globular form. (C) Emission ratio images of the emission intensities of poly(NIPAM-*co*-NBD-*co*-TfAuNC) at 510–560 nm and 570–670 nm in HeLa cells at 25.0, 31.2, 33.0, 36.6, 38.7, and 39.7°C (λ_{ex} = 488 nm). (D) Temperature-dependent emission intensity ratio (R) in a single HeLa cell (n = 5, mean ± SD). Inset: calibration line for intracellular thermometry of HeLa cells using poly(NIPAM-*co*-NBD-*co*-TfAuNC). (E) Changes in intracellular temperature after the chemical stimuli with an ionomycin calcium complex solution (1 μM) that induces a Ca^{2+} burst into cells. Reproduced with permission from Qiao et al. (2015). Copyright 2015 American Chemical Society.

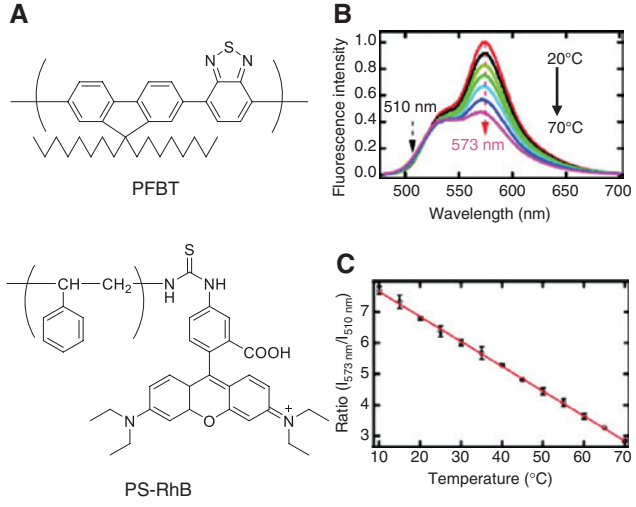

Figure 12: Ratiometric temperature sensing using a combination of PFBT and PS-RhB.
(A) Chemical structures of PFBT and PS-RhB. (B) Fluorescence spectra of a mixture of PFBT and PS-RhB in water (λ_{ex} = 450 nm). (C) Temperature-dependent fluorescence intensity ratio at 573 nm to 510 nm [ratio($I_{573\ nm}/I_{510\ nm}$)]. The error bars represent standard deviation of three independent measurements (n = 3). Reproduced with permission from Ye et al. (2011). Copyright 2011 American Chemical Society.

the temperature-dependent fluorescence properties of the PFBT nanoparticles containing PS-RhB in intracellular spaces.

Europium(III) thenoyltrifluoroacetonate (Eu-TTA) exhibits a temperature-dependent emission intensity due to competition between the luminescence and the non-radiative energy transfer from the Eu^{3+} ion to the ligand (Uchiyama et al. 2006). A ratiometric luminescent nanothermometer (RFNT) was prepared by encapsulating the temperature-sensitive lumophore Eu-TTA and the temperature-insensitive reference fluorophore rhodamine 101 into a cationic nanoparticle (Figure 13A) (Takei et al. 2014). The cationic shell formed using the protonated poly(allylamine) hydrochloride (PAH) supported the incorporation of nanoparticles into the endosomes of HeLa cells via the endocytic pathway. Using the RFNT, heterogeneous heat production in living HeLa cells was observed after a burst of calcium ion influx after ionomycin treatment (Figure 13B and C). The temperature resolution of this nanoparticle was 1.0°C.

A different Eu^{3+} complex [i.e. Eu^{3+}-tris (dinaphthoylmethane)-bis-trioctylphosphine, EuDT] was applied for the temperature mapping of a living organism. It has been suggested that the temperature-dependent luminescent intensity of EuDT at 615 nm was related to the thermal deactivation of both the $^5D_0$ electronic state of Eu^{3+} ion and the triplet excited state of ligands (Peng et al. 2010). The polystyrene-based ratiometric fluorescent luminescent nanoparticle thermosensor (PS-RNT)

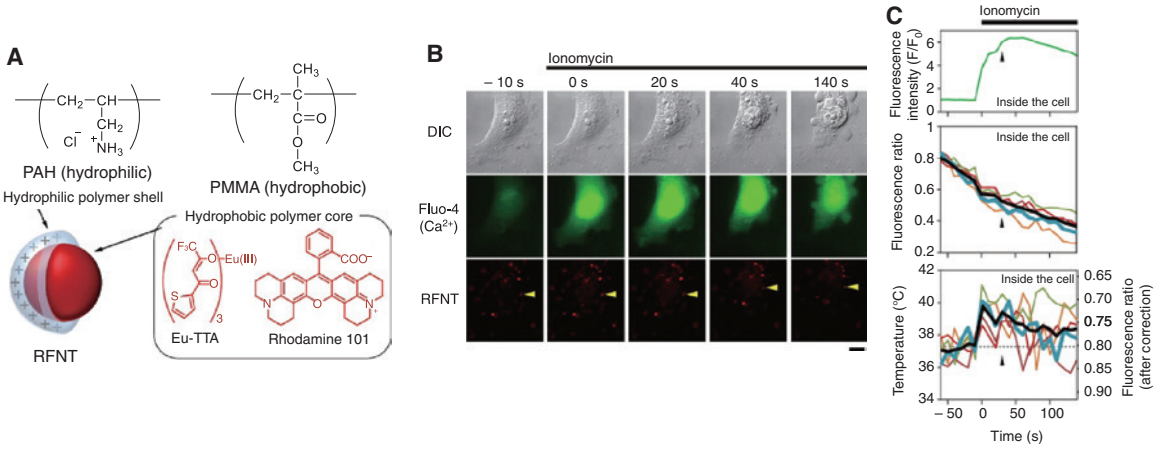

Figure 13: Intracellular thermometry of living HeLa cells using a ratiometric fluorescent nanothermometer (RFNT) containing Eu-TTA and rhodamine 101.
(A) Structure of the RFNT. The hydrophilic shell and hydrophobic core were composed of PAH and poly(methyl methacrylate) (PMMA), respectively. (B) Time lapse imaging of DIC, Fluo-4 (indicating Ca^{2+} ion), and rhodamine 101 in the RFNT after application of the ionomycin-Ca^{2+} complex. (C) Time courses of the fluorescence intensity of Fluo-4 (top), the fluorescence intensity ratio (Eu-TTA/rhodamine 101) of the RFNT (middle), and the evaluated temperature using the fluorescence ratio corrected by cancelling the photobleaching effects. Reproduced with permission from Takei et al. (2014). Copyright 2014 American Chemical Society.

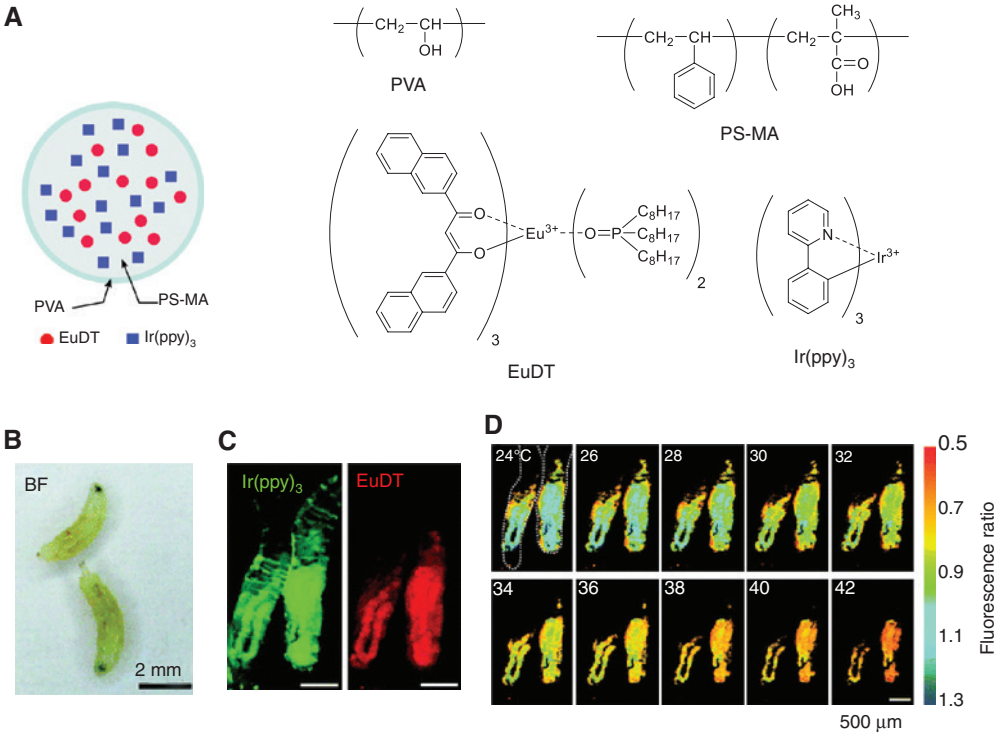

Figure 14: Thermography of fruit fly larvae using polystyrene-based ratiometric fluorescent nanoparticle thermosensor (PS-RNT).
(A) Schematic illustration of PS-RNT and the chemical structures of the components of PS-RNT (i.e. PVA, PS-MA, EuDT, and $Ir(ppy)_3$). (B) Bright field (BF) image of two fruit fly larvae. (C) Fluorescence images of fruit fly larvae obtained under a fluorescence stereomicroscope (λ_{ex} = 405–410 nm). The fruit fly larvae were orally dosed with PS-RNT. Left: $Ir(ppy)_3$ channel (λ_{em} = 520–560 nm). Right: EuDT channel (λ_{em} = 615–624 nm). Scar bar = 500 μm. (D) Thermography of fruit fly larvae using the emission intensity ratio [EuDT/$Ir(ppy)_3$]. Scar bar = 500 μm. Reproduced with permission from Arai et al. (2015). Copyright 2015 Royal Society of Chemistry.

consisted of a poly(styrene-*co*-methacrylic acid) (PS-MA) core, a polyvinylalcohol (PVA) surface, a temperature-sensitive lumophore (i.e. EuDT), and a reference lumophore [i.e. tris(2-phenylpyridinato-C2,N) iridium(III) ($Ir(ppy)_3$)] (Figure 14A) (Arai et al. 2015). The PS-RNT was orally administered to fruit fly larvae (Figure 14B and C).

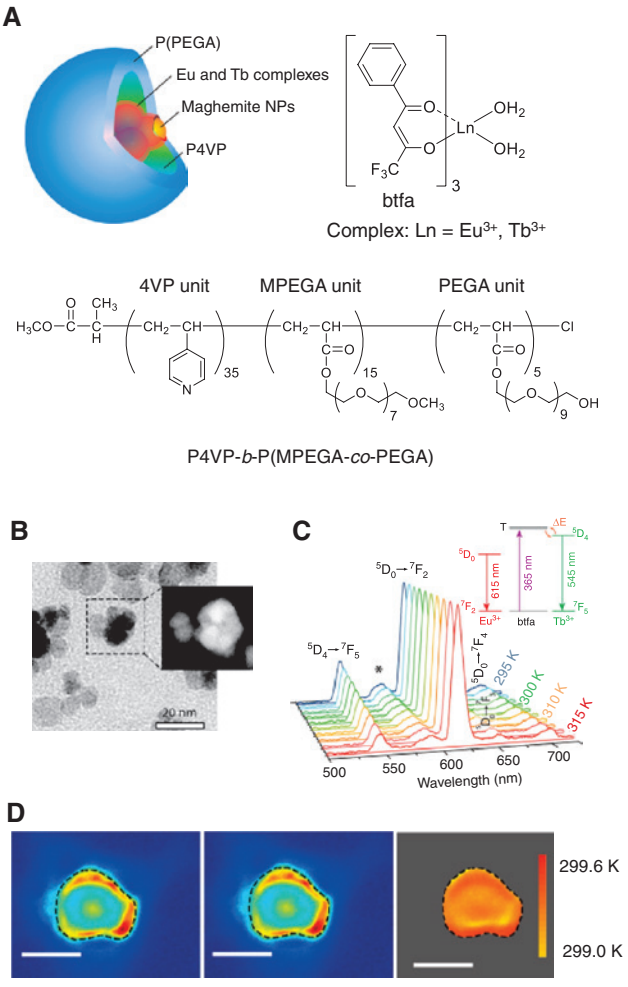

Figure 15: Intracellular temperature mapping of OK cells using maghemite multiparticle core-shell beads.
(A) Schematic representation of a maghemite multiparticle core-shell bead and the chemical structures of its components. (B) TEM/STEM image of the maghemite multiparticle core-shell beads. (C) Emission spectra of the maghemite multiparticle core-shell beads dispersed in water (λ_{ex} = 365 nm). (D) Temperature mapping of an OK cell. Left: Eu^{3+} emission (λ_{em} = 610 nm). Center: Tb^{3+} emission (λ_{em} = 545 nm). Right: pseudocolored temperature map. The interrupted lines delineate the nucleus of the OK cell. Scar bar = 10 µm. Reproduced with permission from Piñol et al. (2015). Copyright 2015 American Chemical Society.

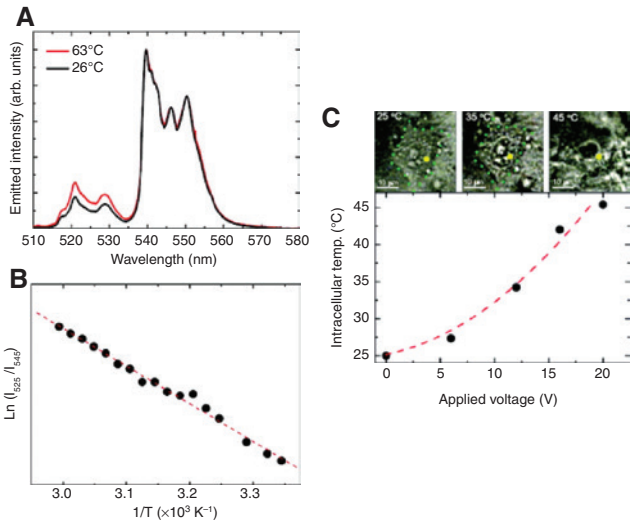

Figure 16: Intracellular temperature sensing using $NaYF_4:Er^{3+},Yb^{3+}$ nanoparticles.
(A) Upconversion emission spectra of $NaYF_4:Er^{3+},Yb^{3+}$ nanoparticles in water (λ_{ex} = 920 nm). (B) Relationship between the emission intensity ratio at 525 and 545 nm [$Ln(I_{525}/I_{545})$] and the temperature. (C) Optical transmission images of a HeLa cell at 25, 35, and 45°C (top) and intracellular temperature of the HeLa cell determined by the incorporated $NaYF_4:Er^{3+},Yb^{3+}$ nanoparticles as a function of the applied voltage (bottom). The temperature of the cell was varied using a metallic platform connected to a resistor by changing the applied voltage. Reproduced with permission from Vetrone et al. (2010). Copyright 2010 American Chemical Society.

Using the emission intensity ratio of EuDT and $Ir(ppy)_3$ as the temperature-dependent parameter, temperature mapping of the fruit fly larvae was performed using the PS-RNT and achieved moderate temperature resolution (1.0–1.7°C) (Figure 14D).

A maghemite multiparticle core-shell bead with the ability to monitor intracellular temperature consisted of Eu^{3+} and Tb^{3+} complexes with 4,4,4-trifluoro-1-phenyl-1,3-butanedione (btfa) ligands, maghemite nanoparticles, a diblock copolymer consisting of 4-vinyl pyridine (4VP) units, methoxy poly(ethylene glycol)acrylate (MPEGA), units and poly(ethylene glycol)acrylate (PEGA) units P4VP-*b*-P(MPEGA-*co*-PEGA)] (Figure 15A and B) (Piñol et al. 2015). The $^5D_4 \rightarrow {}^7F_5$ emission of the Tb^{3+} complex (545 nm) becomes weaker by increasing temperature because the first excited triplet state of the btfa ligand with energy above that of the $^5D_4$ emitting state is likely populated through thermally driven Tb^{3+}-to-ligand energy transfer. In contrast, the $^5D_0 \rightarrow {}^7F_2$ emission of the Eu^{3+} complex (615 nm) is not affected by temperature variations. Therefore, the temperature-dependent emission ratio was obtained from the emissions from the Tb^{3+} and Eu^{3+} complexes (Figure 15C). Although maghemite multiparticle core-shell beads were predominantly located in the nucleus, once incorporated into opossum kidney (OK) cells, temperature mapping of the OK cells was demonstrated using maghemite multiparticle core-shell beads (Figure 15D). Interestingly, this particle also contained ion oxide, which acts as a nanosized chemical heater under magnetic fields. Therefore, this single bead can simultaneously play two independent roles (i.e. a thermometer and a heater), which may enable more precise hyperthermia therapy in cancer treatments.

In the last part in this category, a $NaYF_4:Er^{3+},Yb^{3+}$ nanoparticle is described. This nanoparticle was prepared

from polyethylenimine and contains the $NaYF_4$:Er^{3+},Yb^{3+} dopant as a lumophore (Vetrone et al. 2010). The two radiative excited states ($^2H_{11/2}$: 525 nm and $^4S_{3/2}$: 545 nm) of Er^{3+} in the $NaYF_4$:Er^{3+},Yb^{3+} nanoparticles were thermally equilibrated, and the emission intensity ratio of Er^{3+} at 525 and 545 nm was temperature dependent (Figure 16A and B). After incorporation into the cells, the $NaYF_4$:Er^{3+},Yb^{3+} nanoparticles were used for intracellular thermometry. The temperatures of the HeLa cells that were heated using a voltage-regulated metallic platform were successfully monitored (Figure 16C).

Green fluorescent protein

Luminescent thermometers based on green fluorescent protein (GFP) are highly desirable for biologists because they routinely use GFP for cell analyses. However, GFP typically exhibits only trivial sensitivity to temperature variations.

In 2013, a more sensitive GFP thermometer (i.e. tsGFP1) was developed by combining GFP and the temperature-sensitive protein TlpA, which is derived from the *Salmonella* bacterium (Figure 17A) (Kiyonaka et al. 2013). The temperature-dependent structural changes of TlpA affect the equilibrium of the neutral (–OH) and dissociated ($–O^-$) forms of a hydroxy group in the fluorophore of tsGFP1. The excitation of tsGFP1 in both forms resulted in fluorescence at 510 nm, but the maximum excitation wavelengths were different between the neutral form (at 400 nm) and the dissociated form (at 480 nm). Therefore, the temperature-dependent fluorescence intensity ratios were obtained by excitation at the two different wavelengths, with an emission wavelength fixed at 510 nm (Figure 17B). The use of excitation at two different wavelengths is the unique aspect of the temperature measurements with tsGFP1. Good reversibility in function was confirmed in PBS (Figure 17C). The temperature changes of the endoplasmic reticulum (ER) and mitochondria of HeLa cells were monitored by fusing organelle-targeting sequences to this GFP thermometer. For example, the thermogenesis of a HeLa cell due to a chemical stimulus with an uncoupler agent (carbonyl cyanide 3-chlorophenylhydrazone, CCCP) was observed near the mitochondria (Figure 17D). The changes in the intracellular temperature of brown adipocytes (Figure 17E and F) and myotubes were also imaged.

Quantum dots and carbon dots

Quantum dots have also been utilized for the ratiometric sensing of intracellular temperature due to their remarkable photostability. Recently, it was reported that Qdot 655 nanocrystals exhibit a temperature-dependent shift in the maximum emission wavelength because the temperature affects the lattice of the quantum dots and the

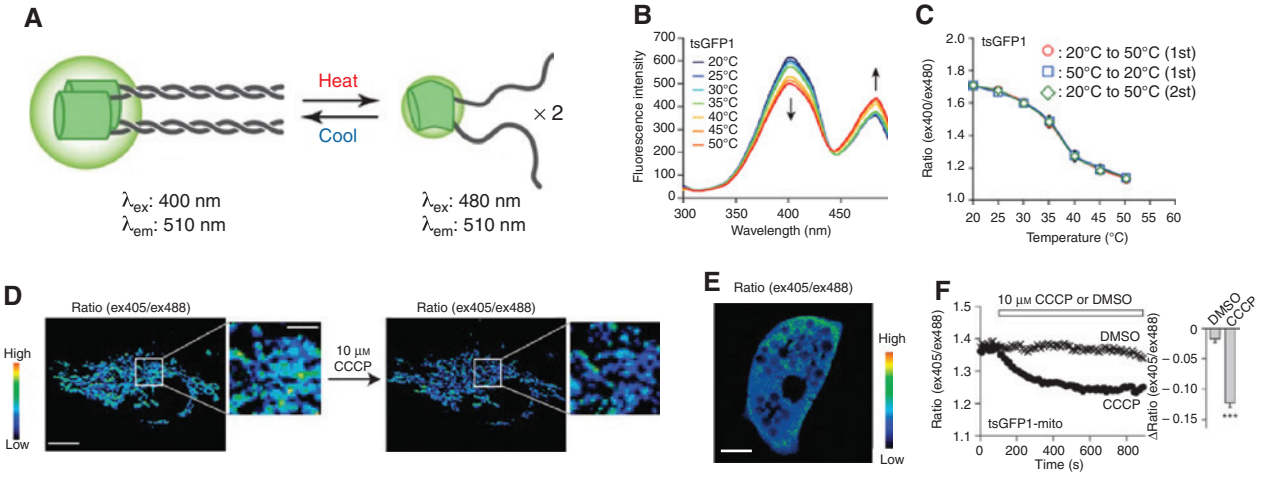

Figure 17: Monitoring of intracellular thermogenesis using a GFP-based thermometer tsGFP1.
(A) Schematic diagram of tsGFP1, which consists of GFP (green) and coiled-coil regions of TlpA (gray). The tandem formation/deformation of the coiled-coil structure upon changes in the temperature resulting in a fluorescence change of tsGFP1. (B) Fluorescence excitation spectra of tsGFP1 in PBS (λ_{em} = 510 nm). (C) Reversibility in the fluorescence intensity ratio of tsGFP1 in PBS. (D) Pseudocolor confocal images of the fluorescence intensity ratio in a HeLa cell expressing mitochondria-targeted tsGFP1 before and after treatment with CCCP. Scar bars = 10 μm (entire image) and 3 μm (enlarged image). (E) Pseudocolor confocal images of the fluorescence intensity ratio in a brown adipocyte expressing mitochondria-targeted tsGFP1. Scar bar = 10 μm. (F) Fluorescence responses of a single brown adipocyte to 10 μM CCCP (n = 28) and DMSO control (n = 24). Left: averaged time courses. Right: changes in the ratio value [Δratio(ex405/ex488)] after CCCP application (mean ± SD). ***$p = 4.8 \times 10^{-6}$ using Student's t-test. Reproduced with permission from Kiyonaka et al. (2013). Copyright 2013 Macmillan Publishers Ltd.

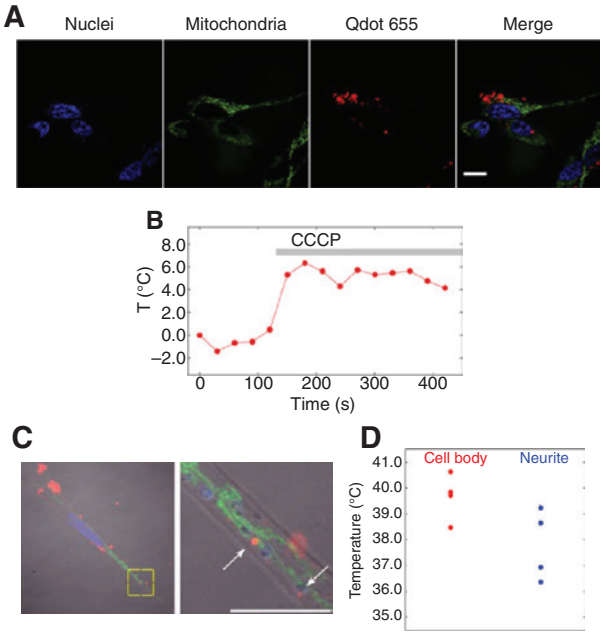

Figure 18: Intracellular thermometry of living cells using Qdot 655 nanocrystals.
(A) Confocal fluorescence images of living SH-SY5Y cells labeling nuclei with Hoechst 33342 (blue) and mitochondria with Mito-Tracker Green FM (green) and incorporating quantum dots (red, λ_{ex} = 405 nm) and their merged image. Scar bar = 20 μm. (B) Change in the temperature near a single Qdot 655 nanocrystal using chemical stimuli with 10 μM CCCP. (C) The merged images of Hoechst 33342 (blue), Mito-Tracker Green FM (green), Qdot 655 nanocrystals (red) and DIC in a neuronal cell. The right image is the enlarged image of the yellow square in the left image. Arrows point to the quantum dots. Scar bar = 10 μm. (D) Temperature difference between the cell body (red) and the neurite (blue) in neuronal cells. The mean difference was 1.6°C (p-value = 0.062). Reproduced from Tanimoto et al. (2016).

electron–lattice interactions (Li et al. 2007), and the emission intensity ratio at 640 nm and 660 nm was temperature dependent (Tanimoto et al. 2016). The Qdot 655 nanocrystals were easily introduced into living SH-SY5Y (human neuroblastoma) cells using a commercially available cell labeling kit (Figure 18A), and the temperature variations of the SH-SY5Y cells after the application of chemical stimuli with CCCP were monitored (Figure 18B). The temperature differences between the cell bodies and the neurites of neuronal cells were also estimated from the temperature-dependent emissions of the Qdot 655 nanocrystals (Figure 18C and D).

A more complex luminescent thermometer based on a CdSe-CdS quantum dot/quantum rod has been reported (Figure 19A) (Albers et al. 2012). A detailed functional mechanism has not been clarified, but it is likely that (i) FRET occurs from the CdSe-CdS quantum dot/quantum rod (ex. 610 nm and em. 625 nm) to a cyanine dye (Alexa-647, ex. 647 nm and em. 675 nm) and (ii) the fluorescence intensity of Alexa-647 decreases with increasing temperature due to the acceleration of the nonradiative photoisomerization process (Widengren and Schwille 2000). This quantum dot/quantum rod-based thermometer was introduced into the cytoplasm of HeLa cells with a cationic polymer colloid. The emission intensity ratio of the quantum dots and Alexa-647 moieties changed as the temperature of the HeLa cells varied (Figure 19B and C).

Carbon dots are new, important photoluminescent materials that are considered less toxic to biorelevant samples and more affordable than quantum dots. Although no studies on carbon dots that exhibit temperature-dependent emission properties have been reported, a nanohybrid of a carbon dot and a temperature-sensitive AuNC has been employed as a ratiometric luminescent thermometer (Wang et al. 2016). The mechanism of temperature-dependent AuNC luminescence is not fully understood, but it is thought that the nonradiative recombination of electrons and holes increases as temperature increases (Bomm et al. 2012). The function

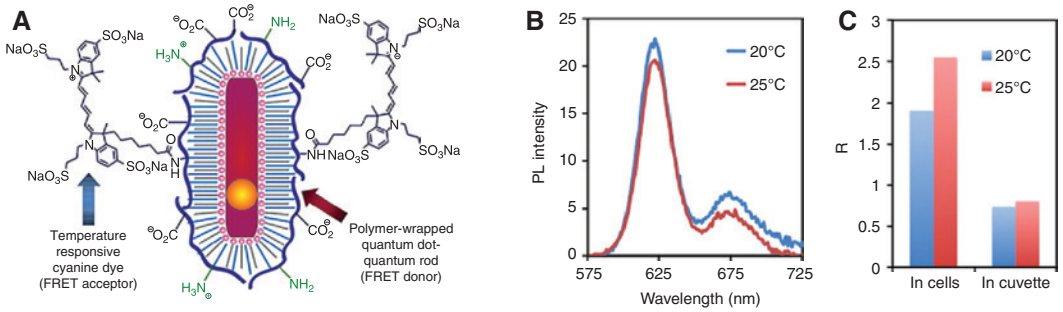

Figure 19: Quantum dot/quantum rod-based nanothermometer for intracellular thermometry.
(A) Chemical structure of the nanothermometer. A red-emitting CdSe-CdS quantum dot/quantum rod semiconductor nanocrystal (center) was passivated with an amphiphilic polymer shell and a far-red emitting cyanine dye. (B) Photoluminescence (PL) spectra in living HeLa cells (λ_{ex} = 400 nm). (C) Photoluminescence intensity ratio ($R = FI_{630–640}/FI_{664–674}$) in living HeLa cells and a 100 mM bicarbonate buffer (pH 8.3). Reproduced with permission from Albers et al. (2012). Copyright 2012 American Chemical Society.

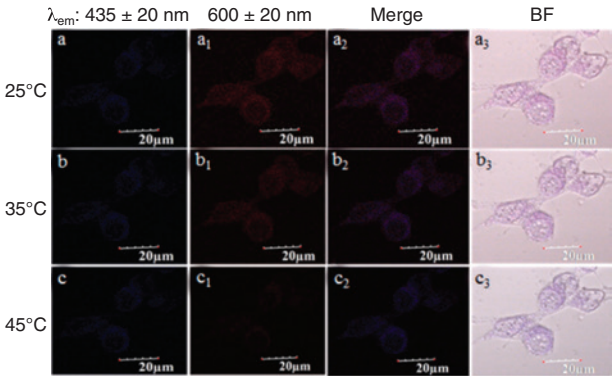

Figure 20: Confocal fluorescence images, merged images and bright-field (BF) images of fixed 293T cells with internalized carbon dot/gold nanocluster hybrids at different temperatures (λ_{ex} = 365 nm). Reproduced with permission from Wang et al. (2016). Copyright 2016 American Chemical Society.

of the nanohybrid was confirmed in fixed HEK293T cells and demonstrated in fluorescence images at different temperatures (i.e. 25, 35, and 45°C) (Figure 20).

Functional independence of ratiometric luminescent molecular thermometers

For accurate temperature measurements inside living cells, the functional independence of ratiometric luminescent molecular thermometers from variations in environmental parameters other than temperature (e.g. pH and ionic strength) should be ensured. Although such

Table 2: Functional independence of the ratiometric luminescent molecular thermometers.

Thermometer	Noneffective environmental factor and tested range	Tested medium	Ref.
Small organic molecules			
Mito-RTP	pH: 4–10 KCl: 0–500 mM	Ethanol-PBS [1:19, v/v]	Homma et al. 2015
Lumophore(s)-labeled thermoresponsive synthetic polymers			
Poly(NNPAM-*co*-APTMA-*co*-DBThD-*co*-BODIPY)	pH: 6–9 KCl: 125–175 mM	150 mM KCl solution or water	Uchiyama et al. 2015
Poly(NNPAM-*co*-APTMA-*co*-Ir_1-*co*-Ir_2)	pH: 4–10 KCl: 50–450 mM BSA[a]	(Not given)	Chen et al. 2016
Poly(NIPAM-*co*-NBD) and poly(NIPAM-*co*-Rh)	pH: 4–9.2 KCl: 0–200 mM BSA[a]	(Not given)	Qiao et al. 2014
PEG-*b*-(NIPAM-*co*-CMA), PEG-*b*-(NIPAM-*co*-NBDAE), and PEG-*b*-(NIPAM-*co*-RhBEA)	pH: 3–9[b]	Water	Hu et al. 2015
Poly(NIPAM-*co*-NBD-*co*-TfAuNC)	pH: 4–8.2 KCl: 50–200 mM BSA: 0–5 mg/l	Water	Qiao et al. 2015
Polymeric materials containing temperature-sensitive lumophores			
Eu-TTA and rhodamine 101 containing RFNT	pH: 4–10 KCl: 0–500 mM BSA: 0–45 wt% Viscosity[c]: 1–220 cP Oxygen: none vs. saturated	PBS or water	Takei et al. 2014
GFP			
tsGFP1	pH: 6.3–8.5 Mg^{2+}: 0–1.2 mM Ca^{2+}: 0–2 mM Dithiothreitol: 0–1 mM Hydrogen peroxide: 0–1 mM	PBS	Kiyonaka et al. 2013
Quantum dots and carbon dots			
Carbon dot/gold nanocluster hybrid	pH: 4–9 Ion: 0–200 mM	(Not given)	Wang et al. 2016

[a]Concentration was not given. [b]Functional independence was confirmed for each polymer. [c]Varied by adding glycerol.

functional independence should be equally demanded of all luminescent sensors, which target even molecules and ions as well as physical parameters, such as temperature and viscosity, this requirement is strictly necessary in luminescent molecular thermometers that are applied to biological cells in particular. As summarized in Table 2, some luminescent molecular thermometers exhibited their functional independence from variations in pH, ionic strength (due to the addition of KCl), viscosity (due to the addition of glycerol), and the concentrations of protein (due to the addition of bovine serum albumin, BSA), Mg^{2+}, Ca^{2+}, reductants (dithiothreitol), oxidants (hydrogen peroxide), and dissolved oxygen in aqueous solution. However, it should be remembered that variations in the above environmental parameters inside cells could depend on the cell lines, and almost no variations in living cells have been quantified, except for limited cases involving pH (Llopis et al. 1998) and viscosity (Liang et al. 2009). Additionally, no current protocol in chemistry can perfectly mimic intracellular environments. Rather, an incredible discrepancy was found between a prepared solution and an intracellular circumstance (Gnutt et al. 2015). Therefore, assessments of functional independence by varying environmental parameters in solution (as indicated in Table 2) are not always sufficient, although they are considered necessary to diminish the possibility of false-positive conclusions. For a more reliable discussion of intracellular temperature, it is preferable to conduct cellular thermometry simultaneously with multiple luminescent molecular thermometers that function via different mechanisms and even with other thermometers, such as a bimaterial (gold and silicon nitride) microcantilevers, although the spatial resolution of such tools is relatively low (Sato et al. 2014).

Closing remarks

The number of luminescent molecular thermometers that have been developed for ratiometric intracellular thermometry has dramatically increased in recent years. In fact, more than half of the thermometers summarized in this review were reported after 2015! Following this trend, we expect that new types of ratiometric luminescent molecular thermometer will continue to be developed. Currently, a variety of ratiometric luminescent molecular thermometers are available, and the appropriate one can be selected for our own research. As indicated in Table 1, some of the ratiometric luminescent molecular thermometers are commercially available, which increases their potential for use.

One future research direction is the development of more sensitive and nontoxic ratiometric luminescent molecular thermometers to pursue their ultimate functions. The comprehension of the functional mechanisms that work in conventional luminescent molecular thermometers should proceed from the viewpoint of photochemistry. Only a few studies on the photophysical processes of luminescent molecular thermometers are available (Gota et al. 2008). In contrast, the reduction of the cytotoxicity of luminescent molecular thermometers requires systematic biological research to correlate the chemical structures of the luminescent molecular thermometers with their cytotoxicities. Accordingly, highly functional thermometers will aid in the elucidation of the temperature profiles of specific cells in more detail. Then, the thermodynamics within a cell could be discussed using imaged intracellular temperature profiles. Some arguments have already been reported in scientific communities (Baffou et al. 2014, Kiyonaka et al. 2015, Suzuki et al. 2015). Another research direction is the correlation of intracellular temperature with numerous cellular events, including pathogenesis. Many laboratories are currently working in this area. Therefore, ratiometric luminescent molecular thermometers will contribute to the establishment of a new academic discipline with the aim of understanding the significance of intracellular temperature.

References

Albers, A. E.; Chan, E. M.; McBride, P. M.; Ajo-Franklin, C. M.; Cohen, B. E.; Helms, B. A. Dual-emitting quantum dot/quantum rod-based nanothermometers with enhanced response and sensitivity in live cells. *J. Am. Chem. Soc.* **2012**, *134*, 9565–9568.

Arai, S.; Ferdinandus, Takeoka, S.; Ishiwata, S.; Sato, H.; Suzuki, M. Micro-thermography in millimeter-scale animals by using orally-dosed fluorescent nanoparticle thermosensors. *Analyst* **2015**, *140*, 7534–7539.

Baffou, G.; Rigneault, H.; Marguet, D.; Jullien, L. A critique of methods for temperature imaging in single cells. *Nat. Methods* **2014**, *11*, 899–901.

Bomm, J.; Günter, C.; Stumpe, J. Synthesis and optical characterization of thermosensitive, luminescent gold nanodots. *J. Phys. Chem. C* **2012**, *116*, 81–85.

Brites, C. D. S.; Lima, P. P.; Silva, N. J. O.; Millán, A.; Amaral, V. S.; Palacio, F.; Carlos, L. D. Thermometry at the nanoscale. *Nanoscale* **2012**, *4*, 4799–4829.

Chapman, C. F.; Liu, Y.; Sonek, G. J.; Tromberg, B. J. The use of exogenous fluorescent probes for temperature measurements in single living cells. *Photochem. Photobiol.* **1995**, *62*, 416–425.

Chen, Z.; Zhang, K. Y.; Tong, X.; Liu, Y.; Hu, C.; Liu, S.; Yu, Q.; Zhao, Q.; Huang, W. Phosphorescent polymeric thermometers for *in vitro* and *in vivo* temperature sensing with minimized background interference. *Adv. Funct. Mater.* **2016**, *26*, 4386–4396.

Gota, C.; Uchiyama, S.; Yoshihara, T.; Tobita, S.; Ohwada, T. Temperature-dependent fluorescence lifetime of a fluorescent polymeric thermometer, poly(*N*-isopropylacrylamide), labeled by polarity and hydrogen bonding sensitive 4-sulfamoyl-7-aminobenzofurazn. *J. Phys. Chem. B* **2008**, *112*, 2829–2836.

Gnutt, D.; Gao, M.; Brylski, O.; Heyden, M.; Ebbinghaus, S. Excluded-volume effects in living cells. *Angew. Chem. Int. Ed.* **2015**, *54*, 2548–2551.

Hattori, K.; Naguro, I.; Okabe, K.; Funatsu, T.; Furutani, S.; Takeda, K.; Ichijo, H. ASK1 signalling regulates brown and beige adipocyte function. *Nat. Commun.* **2016**, *7*, 11158.

Homma, M.; Takei, Y.; Murata, A.; Inoue, T.; Takeoka, S. A ratiometric fluorescent molecular probe for visualization of mitochondrial temperature in living cells. *Chem. Commun.* **2015**, *51*, 6194–6197.

Hu, X.; Li, Y.; Liu, T.; Zhang, G.; Liu, S. Intracellular cascade FRET for temperature imaging of living cells with polymeric ratiometric fluorescent thermometers. *ACS Appl. Mater. Interfaces* **2015**, *7*, 15551–15560.

Inada, N.; Uchiyama, S. Methods and benefits of imaging the temperature distribution inside living cells. *Imaging Med.* **2013**, *5*, 303–305.

Jaque, D.; Vetrone, F. Luminescence nanothermometry. *Nanoscale* **2012**, *4*, 4301–4326.

Kiyonaka, S.; Kajimoto, T.; Sakaguchi, R.; Shinmi, D.; Omatsu-Kanbe, M.; Matsuura, H.; Imamura, H.; Yoshizaki, T.; Hamachi, I.; Morii, T.; Mori, Y. Genetically encoded fluorescent thermosensors visualize subcellular thermoregulation in living cells. *Nat. Methods* **2013**, *10*, 1232–1238.

Kiyonaka, S.; Sakaguchi, R.; Hamachi, I.; Morii, T.; Yoshizaki, T.; Mori, Y. Validating subcellular thermal changes revealed by fluorescent thermosensors. *Nat. Methods* **2015**, *12*, 801–802.

Lee, M. H., Kim, J. S.; Sessler, J. L. Small molecule-based ratiometric fluorescence probes for cations, anions, and biomolecules. *Chem. Soc. Rev.* **2015**, *44*, 4185–4191.

Li, S.; Zhang, K.; Yang, J.-M.; Lin, L.; Yang, H. Single quantum dots as local temperature markers. *Nano Lett.* **2007**, *7*, 3102–3105.

Liang, L.; Wang, X.; Xing, D.; Chen, T.; Chen, W. R. Noninvasive determination of cell nucleoplasmic viscosity by fluorescence correlation spectroscopy. *J. Biomed. Opt.* **2009**, *14*, 024013.

Liu, J.; Guo, X.; Hu, R.; Xu, J.; Wang, S.; Li, S.; Li, Y.; Yang, G. Intracellular fluorescent temperature probe based on triarylboron substituted poly *N*-isopropylacrylamide and energy transfer. *Anal. Chem.* **2015**, *87*, 3694–3698.

Llopis, J.; McCaffery, J. M.; Miyawaki, A.; Farquhar, M. G.; Tsien, R. Y. Measurement of cytosolic, mitochondrial, and Golgi pH in single living cells with green fluorescent proteins. *Proc. Natl. Acad. Sci. USA* **1998**, *95*, 6803–6808.

McCabe, K. M.; Hernandez, M. Molecular thermometry. *Pediatr. Res.* **2010**, *67*, 469–475.

Monti, M.; Brandt, L.; Ikomi-Kumm, J.; Olsson, H. Microcalorimetric investigation of cell metabolism in tumour cells from patients with non-Hodgkin lymphoma (NHL). *Scand. J. Haematol.* **1986**, *36*, 353–357.

Paviolo, C.; Clayton, A. H. A.; Mcarthur, S. L.; Stoddart, P. R. Temperature measurement in the microscopic regime: a comparison between fluorescence lifetime- and intensity-based methods. *J. Microscopy* **2013**, *250*, 179–188.

Peng, H.; Stich, M. I. J.; Yu, J.; Sun, L.-n, Fischer, L. H.; Wolfbeis, O. S. Luminescent europium(III) nanoparticles for sensing and imaging of temperature in the physiological range. *Adv. Mater.* **2010**, *22*, 716–719.

Piñol, R.; Brites, C. D. S.; Bustamante, R.; Martínez, A.; Silva, N. J. O.; Murillo, J. L.; Cases, R.; Carrey, J.; Estepa, C.; Sosa, C.; Palacio, F.; Carlos, L. D.; Millán, A. Joining time-resolved thermometry and magnetic-induced heating in a single nanoparticle unveils intriguing thermal properties. *ACS Nano* **2015**, *9*, 3134–3142.

Qiao, J.; Chen, C.; Qi, L.; Liu, M.; Dong, P.; Jiang, Q.; Yang, X.; Mu, X.; Mao, L. Intracellular temperature sensing by a ratiometric fluorescent polymer thermometer. *J. Mater. Chem. B* **2014**, *2*, 7544–7550.

Qiao, J.; Hwang, Y.-H.; Chen, C.-F.; Qi, L.; Dong, P.; Mu, X.-Y.; Kim, D.-P. Ratiometric fluorescent polymeric thermometer for thermogenesis investigation in living cells. *Anal. Chem.* **2015**, *87*, 10535–10541.

Sato, M. K.; Toda, M.; Inomata, N.; Maruyama, H.; Okamatsu-Ogura, Y.; Arai, F.; Ono, T.; Ishijima, A.; Inoue, Y. Temperature changes in brown adipocytes detected with a bimaterial microcantilever. *Biophys. J.* **2014**, *106*, 2458–2464.

Snare, M. J.; Treloar, F. E.; Ghiggino, K. P.; Thistlethwaite, P. J. The photophysics of rhodamine B. *J. Photochem.* **1982**, *18*, 335–346.

Suzuki, M.; Zeeb, V.; Arai, S.; Oyama, K.; Ishiwata, S. The 10^5 gap issue between calculation and measurement in single-cell thermometry. *Nat. Methods* **2015**, *12*, 802–803.

Uchiyama, S.; Matsumura, Y.; de Silva, A. P.; Iwai, K. Fluorescent molecular thermometers based on polymers showing temperature-induced phase transitions and labeled with polarity-responsive benzofurazans. *Anal. Chem.* **2003**, *75*, 5926–5935.

Uchiyama, S.; de Silva, A. P.; Iwai, K. Luminescent molecular thermometers. *J. Chem. Educ.* **2006**, *83*, 720–727.

Uchiyama, S.; Tsuji, T.; Ikado, K.; Yoshida, A.; Kawamoto, K.; Hayashi, T.; Inada, N. A cationic fluorescent polymeric thermometer for the ratiometric sensing of intracellular temperature. *Analyst* **2015**, *140*, 4498–4506.

Uchiyama, S.; Inada, N. Cellular thermometry. In Thermometry at the Nanoscale: Techniques and Selected Applications. Carlos, L. D.; Palacio, F., Eds. Royal Society of Chemistry: Cambridge; 2016; pp. 355–382.

Takei, Y.; Arai, S.; Murata, A.; Takabayashi, M.; Oyama, K.; Ishiwata, S.; Takeoka, S.; Suzuki, M. A nanoparticle-based ratiometric and self-calibrated fluorescent thermometer for single living cells. *ACS Nano* **2014**, *8*, 198–206.

Tanimoto, R.; Hiraiwa, T.; Nakai, Y.; Shindo, Y.; Oka, K.; Hiroi, N.; Funahashi, A. Detection of temperature difference in neuronal cells. *Sci. Rep.* **2016**, *6*, 22071.

Valeur, B.; Berberan-Santos, M. N. Molecular Fluorescence–Principles and Applications; 2nd Edition. Wiley-VCH: Weinheim, 2012; pp. 411–412.

Vetrone, F.; Naccache, R.; Zamarrón, A.; de la Fuente, A. J.; Sanz-Rodríguez, F.; Maestro, L. M.; Rodriguez, E. M.; Jaque, D.; Solé, J. G.; Capobianco, J. A. Temperature sensing using fluorescent nanothermometers. *ACS Nano* **2010**, *4*, 3254–3258.

Wang, X.-d.; Wolfbeis, O. S.; Meier, R. J. Luminescent probes and sensors for temperature. *Chem. Soc. Rev.* **2013**, *42*, 7834–7869.

Wang, C.; Lin, H.; Xu, Z.; Huang, Y.; Humphrey, M. G.; Zhang, C. Tunable carbon-dot-based dual-emission fluorescent nanohybrids

for ratiometric optical thermometry in living cells. *ACS Appl. Mater. Interfaces* **2016**, *8*, 6621–6628.
Widengren, J.; Schwille, P. Characterization of photoinduced isomerization and back-isomerization of the cyanine dye Cy5 by fluorescence correlation spectroscopy. *J. Phys. Chem. A* **2000**, *104*, 6416–6428.
Ye, F.; Wu, C.; Jin, Y.; Chan, Y.-H.; Zhang, X.; Chiu, D. T. Ratiometric temperature sensing with semiconducting polymer dots. *J. Am. Chem. Soc.* **2011**, *133*, 8146–8149.

Bionotes

Seiichi Uchiyama
Graduate School of Pharmaceutical Sciences, The University of Tokyo, 7-3-1 Hongo Bunkyo-ku, 113-0033 Tokyo, Japan,
seiichi@mol.f.u-tokyo.ac.jp

Seiichi Uchiyama received his BS, MS, and PhD degrees in Pharmacy from the University of Tokyo. Then, he spent 3 years as a postdoctoral researcher in Nara Women's University (supervisor: Prof. Kaoru Iwai) and Queen's University of Belfast (supervisor: Prof. A. Prasanna de Silva). After returning to the University of Tokyo in 2005, he started his career as an experimental researcher and continues to work as a leader of scientific projects funded by the Japanese government. His current interests include analytical and photophysical chemistry, horseracing, and eating.

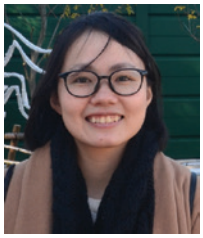

Chie Gota
Graduate School of Pharmaceutical Sciences, The University of Tokyo, 7-3-1 Hongo Bunkyo-ku, 113-0033 Tokyo, Japan

Chie Gota received her BS and MS degrees in Pharmacy from the University of Tokyo. After finishing her MS course in 2008, she started working in a Japanese cosmetic company (KOSÉ Corporation) as a researcher. In 2013, she was awarded the Best Paper Prize from the Society of Cosmetic Chemists of Japan. Since 2015, she has been involved in collaborative research with Dr. Uchiyama on the development of novel functional polymeric materials. She enjoys polymer chemistry, singing and magic.